Supplemental Materials for

Loss of *CLN3*, the gene mutated in juvenile neuronal ceroid lipofuscinosis, leads to metabolic impairment and autophagy induction in retina pigment epithelium

Yu Zhong[3], Kabhilan Mohan[1,9], Jinpeng Liu[2], Ahmad Al-Attar[4], Penghui Lin[4], Robert M. Flight[2,4], Qiushi Sun[4,10], Marc O. Warmoes[4,11], Rahul R. Deshpande[4], Huijuan Liu[3], Kyung Sik Jung[1,9], Mihail I. Mitov[2,12], Nianwei Lin[13,14], D. Allan Butterfield[2,5], Shuyan Lu[13], Jinze Liu[2,6,7], Hunter N. B. Moseley[2,3,7], Teresa W. M. Fan[2,4,8], Mark E. Kleinman[1,9], Qing Jun Wang[1,2,*]

[1] Department of Ophthalmology and Visual Sciences

[2] Markey Cancer Center

[3] Department of Molecular and Cellular Biochemistry

[4] Center for Environment and Systems Biochemistry

[5] Department of Chemistry

[6] Department of Computer Science

[7] Institute for Biomedical Informatics

[8] Department of Toxicology and Cancer Biology

University of Kentucky, Lexington, KY, United States

[9] Current Address: Department of Surgery, East Tennessee State University, Johnson City, TN, United States

[10] Current Address: Department of Internal Medicine/Endocrinology, Yale School of Medicine, New Haven, CT, United States

[11] Current Address: Luxembourg Centre for Systems Biomedicine, University of Luxembourg, Belvaux, Luxembourg

[12] Current Address: Idaho College of Osteopathic Medicine, Meridian, ID, United States

[13] Pfizer Inc., San Diego, CA, United States

[14] Current Address: iXCells Biotechnologies USA, Inc., San Diego, CA, United States

* Correspondence: Department of Ophthalmology and Visual Sciences, University of Kentucky, Lexington, KY 40536. Email: qingjun.wang@uky.edu.

Supplemental Methods

Toluidine blue stain

Toluidine Blue stains acidic tissue components. It has a high affinity for nucleic acids and therefore stains DNA- and RNA-rich nuclear compartments within tissues. It also stains polysaccharides violet or purple. Semi-thin (1.5-2 μm) sections of resin-embedded retinas (described in **Experimental Procedures**) were cut and stained with 1:1 mix of 0.5% Toluidine blue and 0.25% sodium borate (both in ddH_2O) on a hot plate at medium heat for 30 sec to 1 min. Rinse each section with ddH_2O and let it dry on the hot plate before mounting the slide.

Quantitative real time PCR

Quantitative real time PCR (qRT-PCR) was performed as described previously (Zhong et al., 2014). In brief, RPE-1 cells that were reverse-transfected respectively with non-targeting, CLN3 exon-6, and CLN3 exon-8 siRNA were seeded into 60-mm dishes and cultured for 48 h before cells were harvested. Total mRNAs were extracted from each sample using TRIzol (Thermo Fisher Scientific 15596018), following the manufacturer's instructions. Purified total mRNAs (1 μg) from each sample were converted to cDNAs in 20-μl reaction mixtures using the iScript™ cDNA synthesis kit, following the protocols of the manufacturer. Relative amount of mRNAs of any gene of interest was determined by SYBR Green PCR kit (Bio-rad) on a Stratagene Mx3005P QPCR system (Agilent Technologies), using primer pairs specific to that gene. Primers used for qRT-PCR are listed in **Supplemental Table 3** (Integrated DNA Technologies). Three replicates were performed for each primer pair-gene combination. Actin mRNAs were used as the internal controls. Levels of all qRT-PCR amplified products were normalized to the actin qRT-PCR amplicon levels.

Supplemental Tables

Supplemental Table 1. Whole list of the result from the differential expression analysis of the RNA-Seq data comparing CLN3 siRNA-treated versus non-targeting siRNA-treated control RPE-1 cells.

Supplemental Table 2. Whole list of the result from the GSEA analysis of the RNA-Seq data comparing CLN3 siRNA-treated versus non-targeting siRNA-treated control RPE-1 cells. GSEA analysis was done on the C5: GO Gene Set database (total 3600 genes).

Supplemental Table 3. The list of all primers used for qRT-PCR of human autophagy-lysosomal genes. All primers were purchased from Integrated DNA Technologies.

Supplemental Figure Legends

Supplemental Figure 1. Homozygous Cln3$^{\Delta ex7/8}$ mice show vision impairment.

(**A**) Representative scotopic electroretinograms (ERGs) of young WT (10-month old) and homozygous *Cln3$^{\Delta ex7/8}$* (8-month old) mice at increasing light intensity. (**B**) The scotopic ERG b-wave amplitude and a-wave amplitude ratio for both young and old WT and homozygous *Cln3$^{\Delta ex7/8}$* mice at high light intensities 0.63 and 10 cd•s/m^2. The b/a amplitude ratios in both young and old *Cln3$^{\Delta ex7/8}$* mice have a decreasing trend as compared to those in WT mice at comparable ages, even though the difference did not reach statistical significance.

Supplemental Figure 2. The retina of a 22-month old homozygous Cln3$^{\Delta ex7/8}$ mouse shows RPE atrophy and degeneration as well as a large drusen.

(**A**) A Toluidine blue (TB) stained semi-thin section of a 22-month old homozygous *Cln3$^{\Delta ex7/8}$* mouse retina shows a large drusen (marked by a red asterisk in the center of the image). Note that the outer and inner retinal layers as well as the ganglion cell layer appear largely normal. (**B**) Additional electron micrographs showing RPE atrophies, including disintegrated RPE (**left panel**) and RPE metaplasia/hyperplasia (**right panel**) in the 22-month old homozygous *Cln3$^{\Delta ex7/8}$* mouse retina. Scale bars: 2 μm. (**C**) Electron micrographs showing the ultrastructure of different regions of the drusen in (**A**). Note that the middle region (**middle panel**) of this drusen accumulated numerous small vesicular structures of diameter <500 nm, and the basal (**left panel**) and apical (**right panel**) regions contained larger membranous structures which enclosed mitochondria and numerous small vesicular structures. Scale bars are indicated in the figures.

Supplemental Figure 3. CLN3 immunoblot from a whole gel.

(**A**) CLN3 immunoblot from a whole gel for **Figure 2B** shows that CLN3 protein migrated at 64-76 kDa. (**B**) With a longer exposure time for the film, the smearing of CLN3 bands in the same CLN3 immunoblot as in (**A**) was apparent comparing to other bands, consistent with reported tissue-dependent glycosylation and slower migration of the CLN3 protein (Ezaki et al., 2003).

Supplemental Figure 4. Quantitative real time PCR of selected autophagy gene transcripts in CLN3 versus non-targeting siRNA-treated RPE-1 cells.

Quantitative RT-PCR shows up-regulation of (**B**) *p62/SQSTM1*, (**C**) *ULK1*, (**D**) *BECN1*, (**E**) *ATG14*, (**G**) *VPS34/PIK3C3*, (**H**) *VPS15/PIK3R4*, (**I**) *WIPI2*, (**J**) *ATG7*, (**K**) *MAP1BLC3B*, (**L**) *GABARAP* and down-regulation of (**A**) *CLN3* and (**F**) *NRBF2* in CLN3 (versus non-targeting) siRNA-treated RPE-1 cells, consistent with autophagy induction. Statistics: two-tailed t-test with two-sample unequal variance; **, $p<0.05$; *, $0.05<p<0.105$. n=2 for CLN3; n=4 for p62/SQSTM1; and n=3 for all other genes.

Supplemental Figure 5. Quantitative real time PCR of selected CLN and lysosome gene transcripts in non-targeting versus CLN3 siRNA treated RPE-1 cells.

Quantitative RT-PCR shows up-regulation of (**A**) *CLN1/PPT1*, (**B**) *CLN2/TPP1*, (**C**) *CLN5*, (**F**) *CLN10/CTSD*, (**G**) *ATP6V1G1*, (**H**) *LAMP1*, (**I**) *SLC17A5* and down-regulation of (**D**) *CLN6* and (**E**) *CLN8* in CLN3 (versus non-targeting) siRNA-treated RPE-1 cells, consistent with specific enhancement of the lysosomal system. Statistics: two-tailed t-test with two-sample unequal variance; **, $p<0.05$; *, $0.05<p<0.16$. n=3 for all genes.

Supplemental Figure 6. Loss of CLN3 led to decreased $^{13}C_6$-glucose uptake, and decreased excretion of ^{13}C-labeled lactate and pyruvate from NMR analyses of growth media.

(**A-B**) ^{1}H NMR spectra and (**C**) $^{1}H\{^{13}C\}$-HSQC NMR spectra of growth media show more $^{13}C_6$-glucose and less $^{13}C_3$-lactate in the media collected from the CLN3 exon8 siRNA-treated RPE-1 cells (in red) than from the non-targeting siRNA-treated control cells (in black) at 24 h after addition of 25 mM $^{13}C_6$-glucose. Corresponding spectra at 0 h (*i.e.*, the beginning of the labeling) were in light red (for CLN3-deficient cells) and in grey (for non-targeting siRNA treated control cells). Note that light red and grey spectra are mostly overlapping except for the H_2O region. (**D-F**) $^{1}H\{^{13}C\}$-HSQC NMR analyses of growth media at 24 h after $^{13}C_6$-glucose labeling, as compared to right before labeling, show that CLN3-deficient RPE-1 cells had decreased (**D**) $^{13}C_6$-glucose uptake, and decreased production and/or excretion of (**E**) $^{13}C_3$-lactate and (**F**) $^{13}C_3$-pyruvate. Metabolites amounts were normalized by protein amounts of corresponding samples. Due to limit of resources, the SIRM experiment only included single unlabeled sample and duplicated labeled samples for either non-targeting or CLN3 exon-8 siRNA treatment. For

all SIRM quantification results (**D-F**), means and standard errors were plotted for labeled samples.

Supplemental Figure 7. Loss of CLN3 led to increased intracellular glucose levels, as well as decreased intracellular alanine, fumarate, aspartate levels from NMR analyses of RPE-1 cells. $^{1}H\{^{13}C\}$-HSQC NMR analyses of polar extracts of the cells at 24 h after $^{13}C_6$-glucose labeling show that CLN3-deficient RPE-1 cells had (**A**) increased intracellular levels of $^{13}C_6$-glucose and (**B**) decreased intracellular levels of $^{13}C_3$-alanine. $^{1}H\{^{13}C\}$-HSQC NMR spectra were acquired for labeled samples only. ^{1}H NMR analyses of RPE-1 cell extract polar fractions show decreased levels of (**C**) unlabeled fumarate and (**D**) unlabeled aspartate upon CLN3 deficiency. Metabolites amounts were normalized by protein amounts of corresponding samples. Due to limit of resources, the SIRM experiment only included single unlabeled sample and duplicated labeled samples for either non-targeting or CLN3 exon-8 siRNA treatment. For all SIRM quantification results (**A-D**), means and standard errors were plotted for labeled samples.

Supplemental Figure 8. Loss of CLN3 led to decreased ^{13}C enrichment in several lipid classes. This figure shows fractional enrichment of ^{13}C in the lipids present in the non-polar extracts of 24 h $^{13}C_6$-glucose-fed CLN3-deficient RPE-1 cells. Direct infusion FTICR-MS of non-polar cell extracts detected decreased fractional enrichment of even-number ^{13}C-labeled (**A**) sphingomyelins (SM), (**B**) triacylglycerols (TAG), (**C**) phosphatidylcholines (PC), and (**D**) phosphatidylethanolamines (PE) in CLN3 (versus non-targeting) siRNA-treated RPE-1 cells. Note that lack of m3 isotopologues of SM is consistent with SM not having a glycerol backbone. Metabolites amounts were normalized by protein amounts of corresponding samples. Due to limit of resources, the SIRM experiment only included single unlabeled sample and duplicated labeled samples for either non-targeting or CLN3 exon-8 siRNA treatment. For all SIRM quantification results (**A-D**), means and standard errors were plotted for labeled samples.

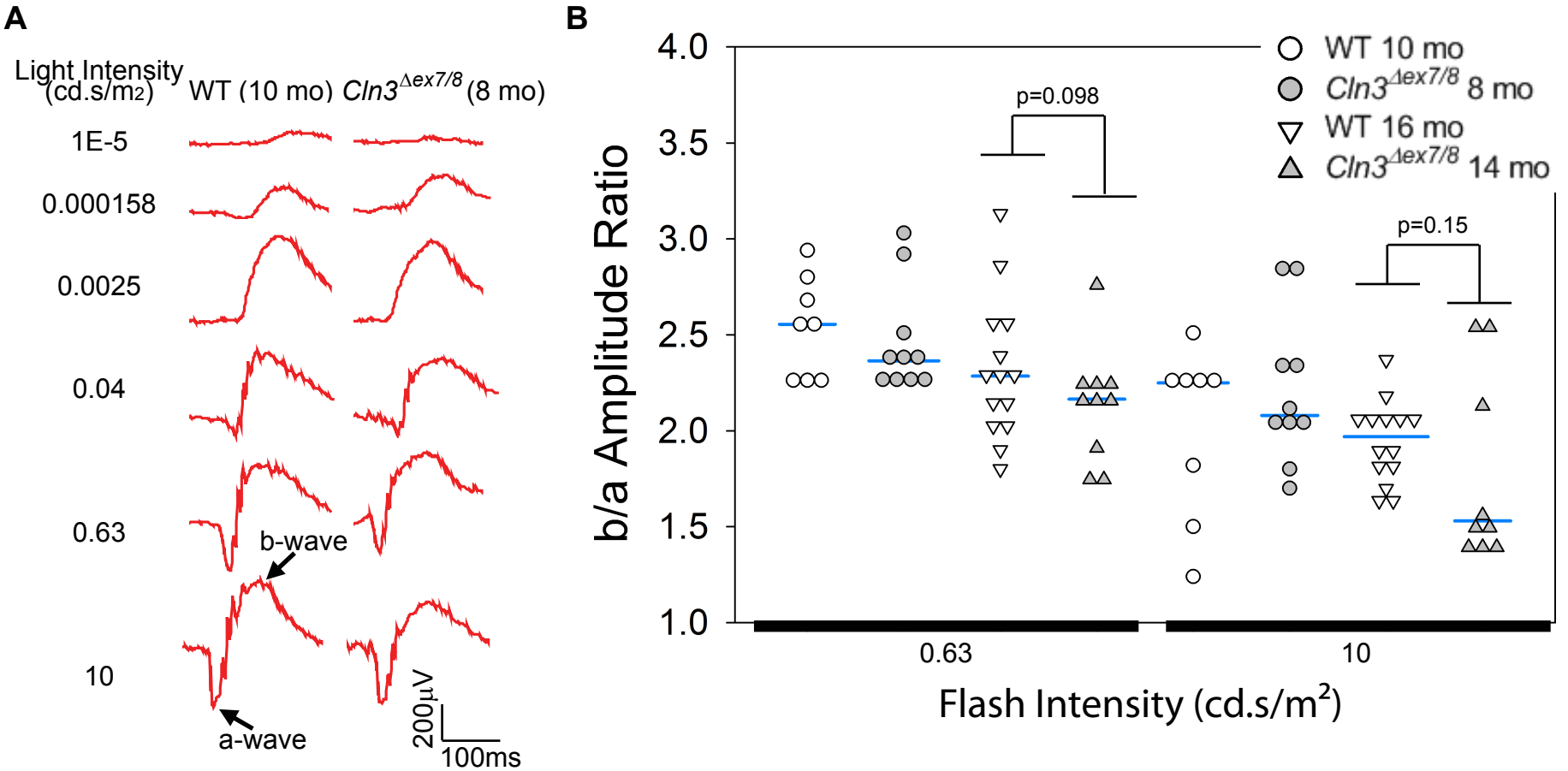

Supplemental Figure 1

Supplemental Figure 2

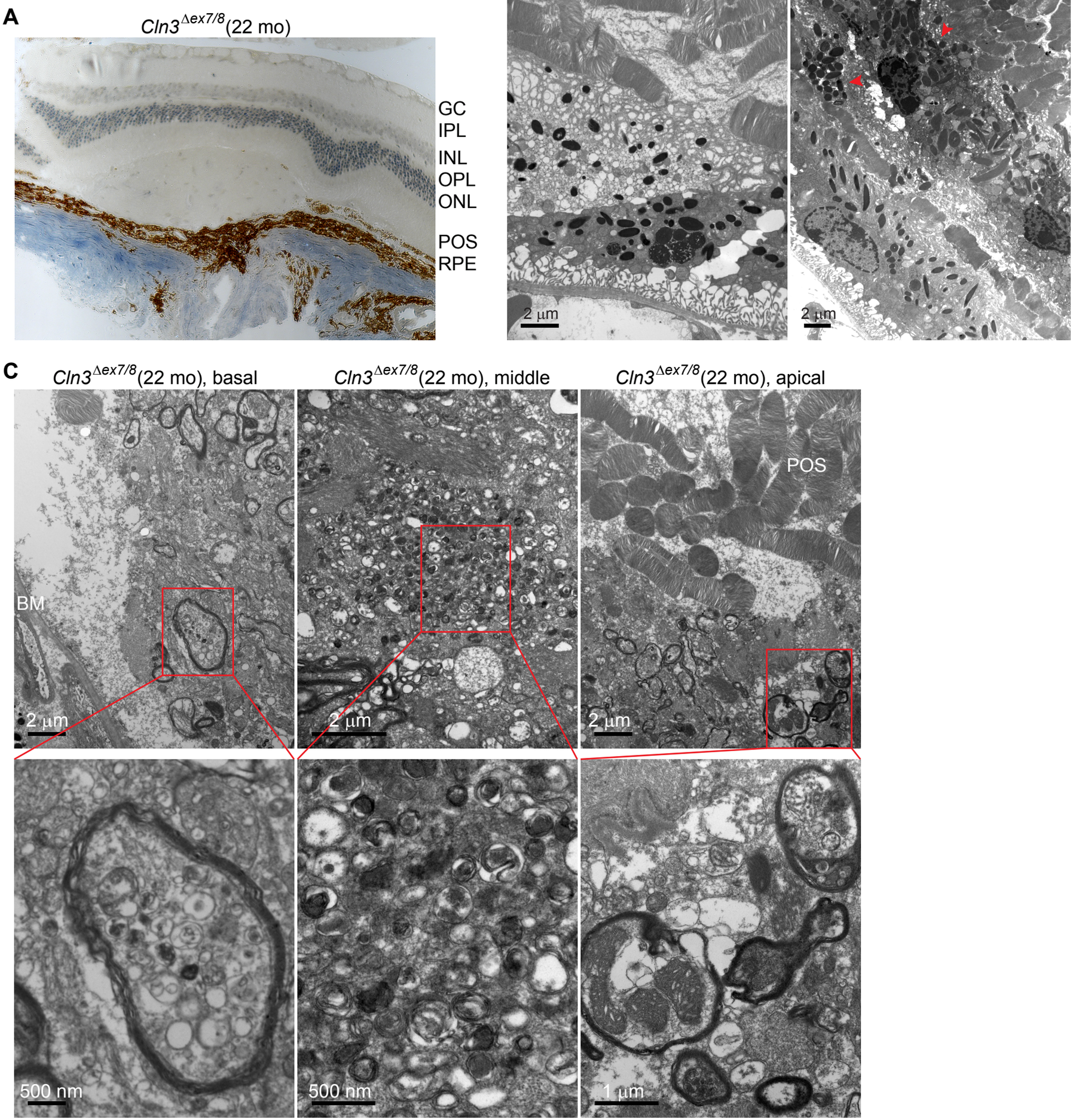

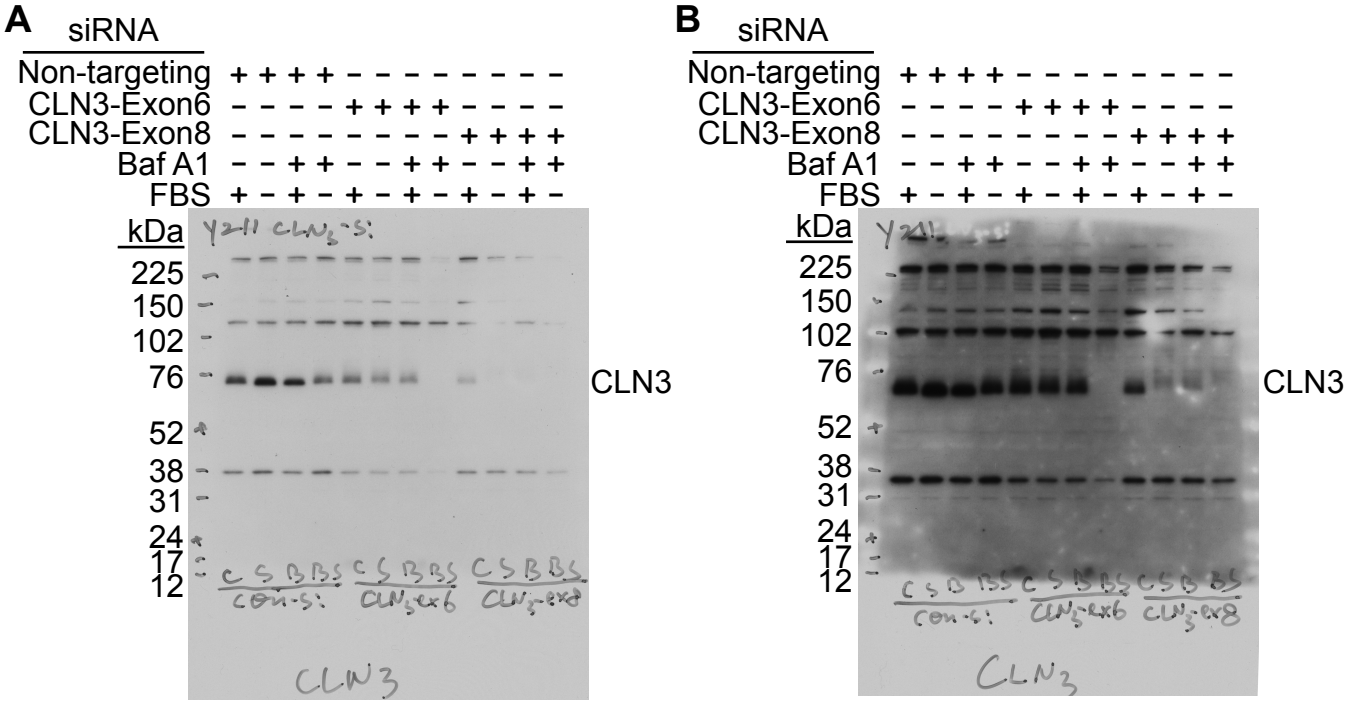

Supplemental Figure 3

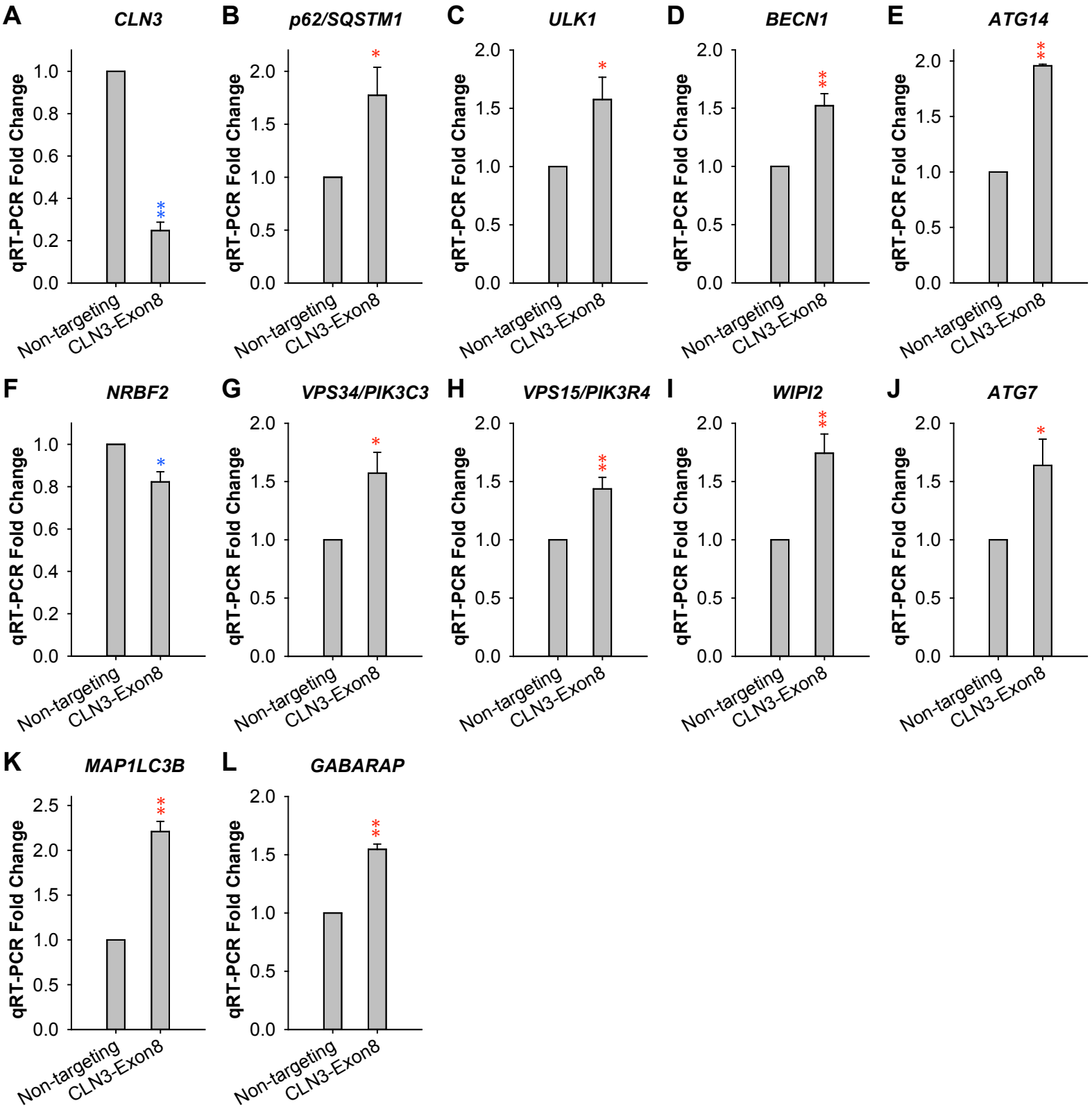

Supplemental Figure 4

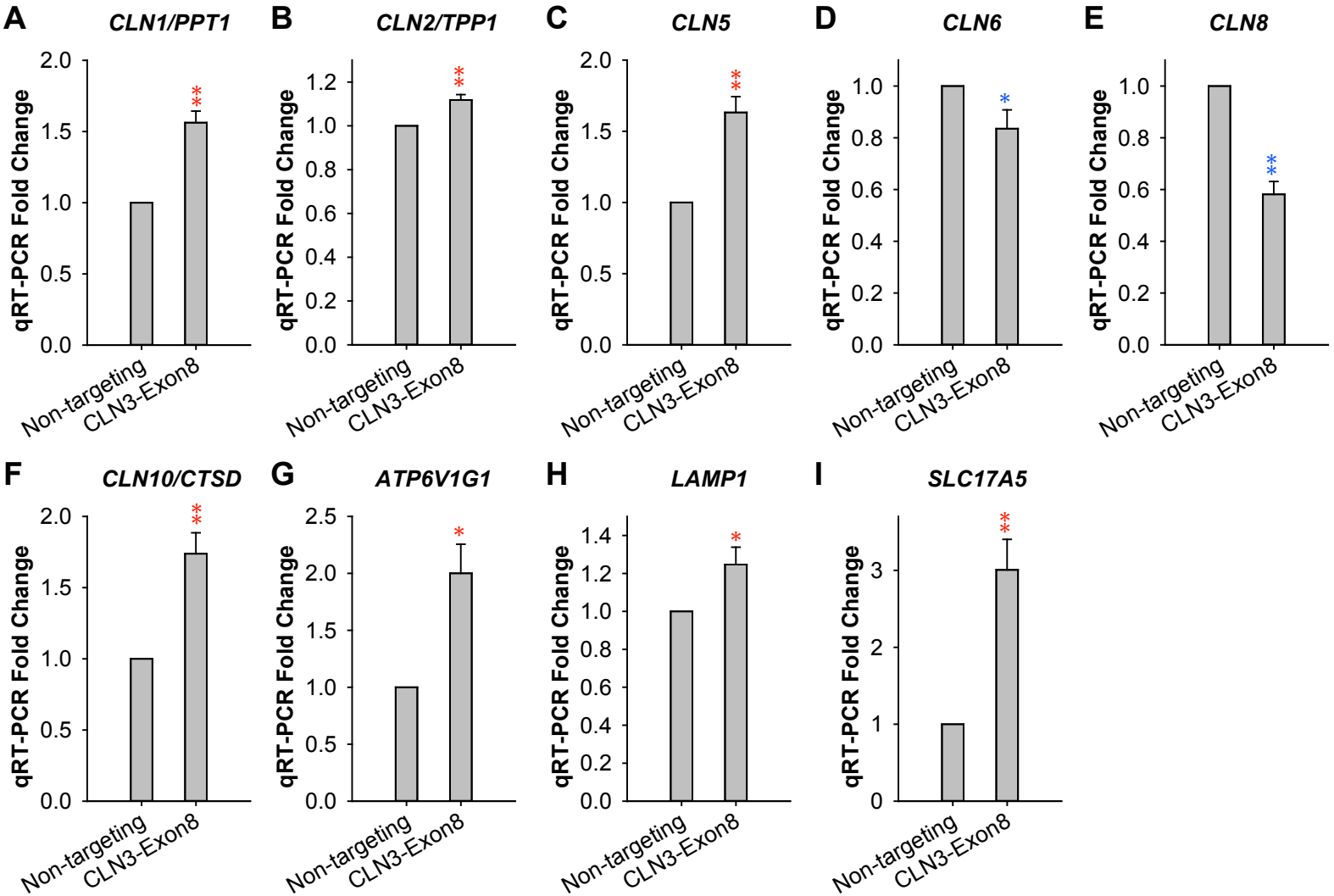

Supplemental Figure 5

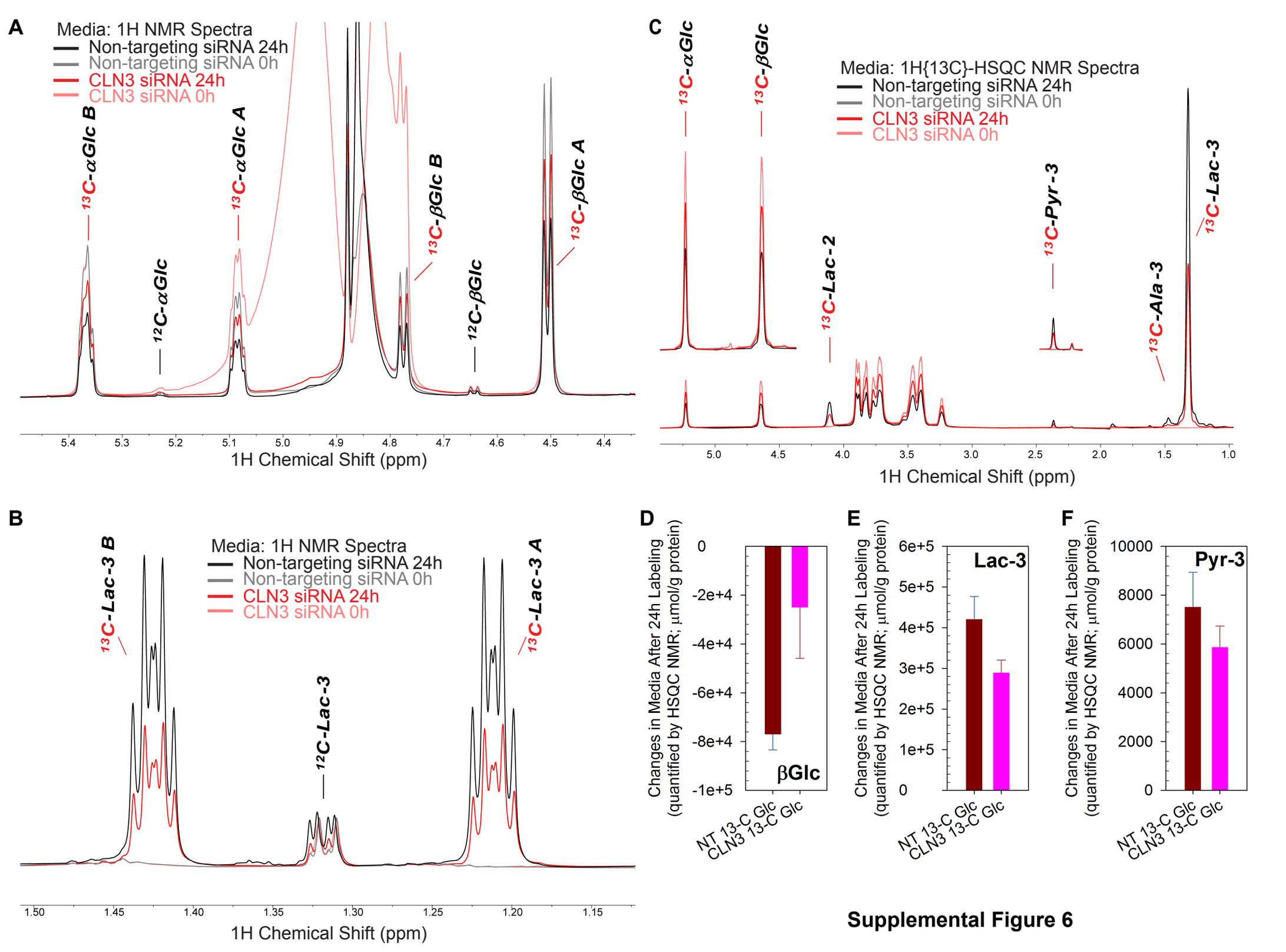

Supplemental Figure 6

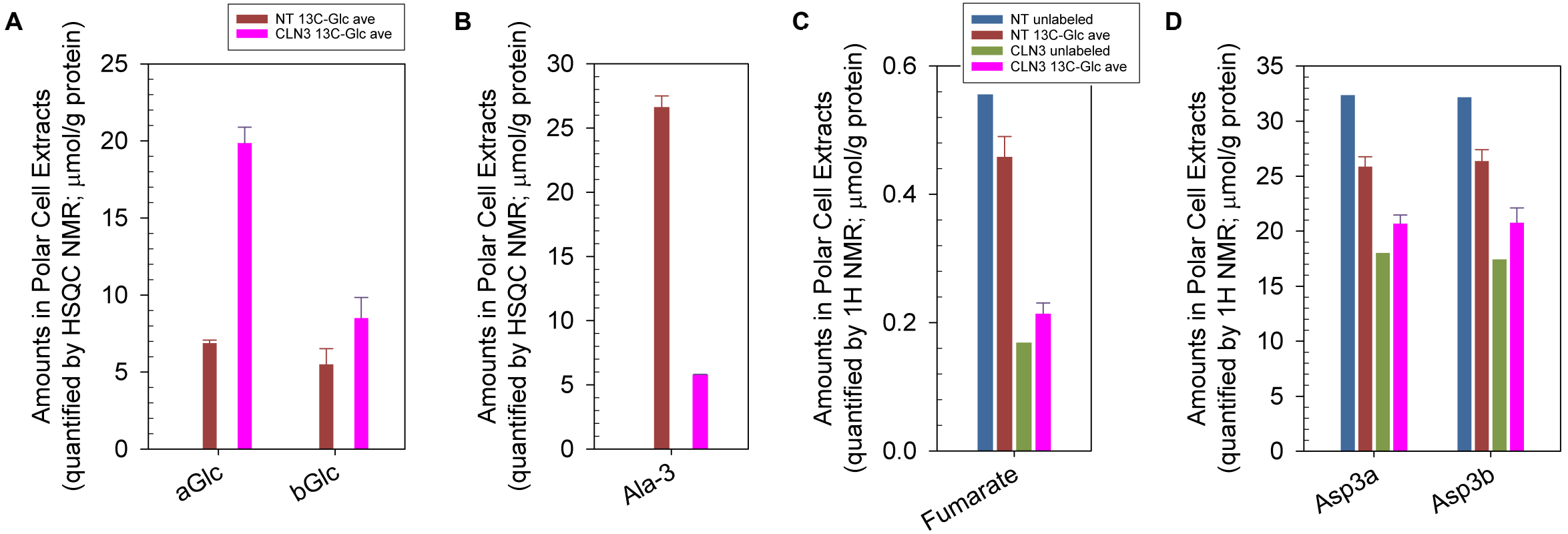

Supplemental Figure 7

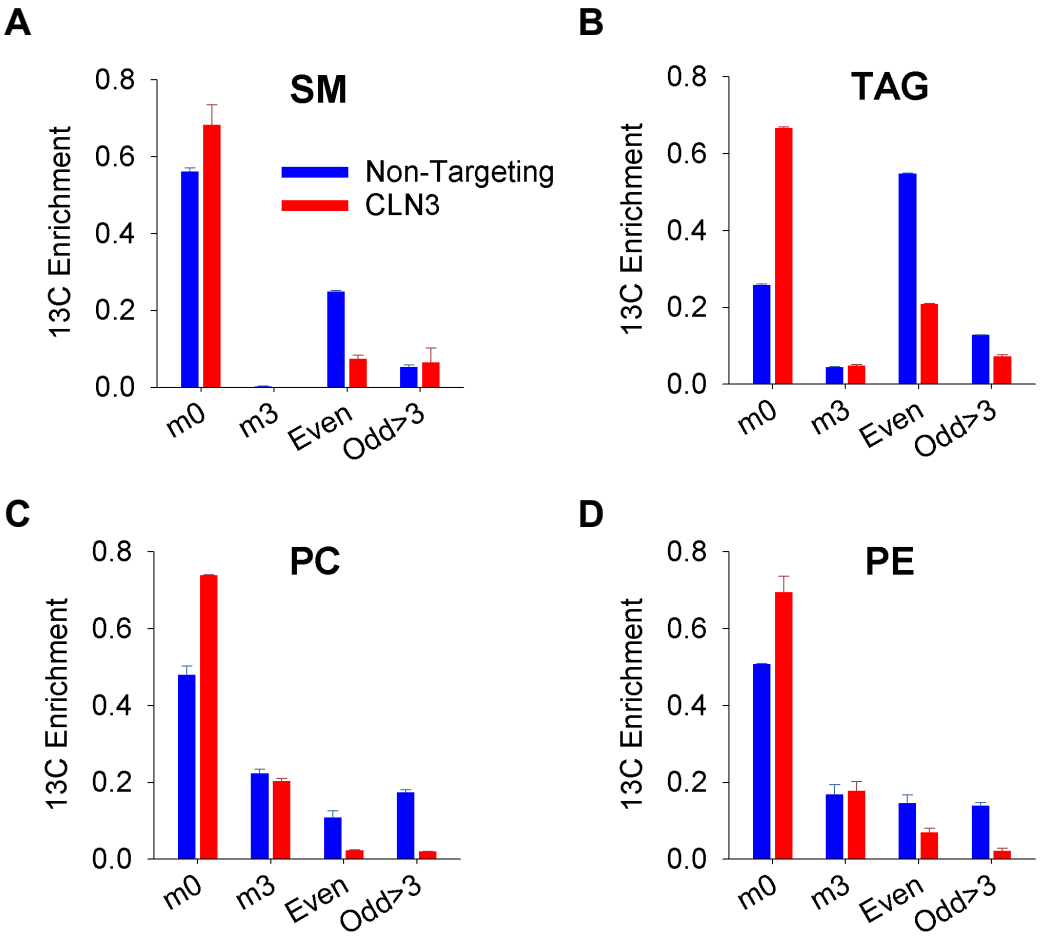

Supplemental Figure 8